DIAGNOSTYKA, 2026, Vol. 27, No. 3

e-ISSN 2449-5220
DOI: 10.29354/diag/231242

DEEP LEARNING-DRIVEN INTELLIGENT DIAGNOSTIC SYSTEM FOR ELECTROMECHANICAL EQUIPMENT FAILURES

Ting FU

Changjiang Polytechnic, Wuhan, Hubei, 430074, China
Corresponding author, e-mail: futingtf8@outlook.com

Abstract

The objective of this research is to design a deep learning-driven intelligent diagnostic system for electromechanical equipment failures, introducing a novel framework termed OPS-DC-LSTM-AE. The Electromechanical Fault Dataset contains 2,300 labeled samples combining vibration, current, and acoustic features for diagnosing faults under varied operating conditions. Pre-processing is achieved through adaptive noise reduction using wavelet packet decomposition, ensuring cleaner signals. For feature extraction, the FFT is applied to capture both temporal and frequency-domain characteristics. The proposed framework integrates OPS to optimize hyperparameters of the DC-LSTM-AE model. The Convolutional layers capture localized signal features, the LSTM layers model temporal dependencies, while the AutoEncoder ensures dimensionality reduction and latent feature learning. This synergy yields an intelligent system capable of diagnosing both single and compound faults with enhanced precision. Results demonstrate superior accuracy of 98.12% and an F1-score of 98.11% using a Python-implemented model, outperforming conventional deep learning approaches. In conclusion, the OPS-DC-LSTM-AE model establishes a powerful and adaptive diagnostic framework, advancing fault detection capabilities in electromechanical equipment toward intelligent and reliable operations.

Keywords: electromechanical equipment, fault diagnosis, intelligent diagnostic system, predictive maintenance, orca predation search-driven deep convolutional-long short-term memory with autoencoder (OPS-DC-LSTM-AE)

List of Symbols/Acronyms

Abbreviation / Symbol	**Full Form**
OPS	Orca Predation Search
OPS-DC-LSTM-AE	Orca Predation Search-driven Deep Convolutional-Long Short-Term Memory with AutoEncoder
DC	Deep Convolutional
LSTM	Long Short-Term Memory
LSTM-AE	Long Short-Term Memory with AutoEncoder
AE	AutoEncoder
SSA-BiGRU-Attention	Sparrow Search Algorithm–Bidirectional Gated Recurrent Unit with Attention
CPL	Curriculum Pseudo Labeling
2D-CNN	Two-Dimensional Convolutional Neural Network
SFUDA	Source-Free Unsupervised Domain Adaptation
ECAAE	Extended Convolutional Adversarial AutoEncoder
MAE	Mean Absolute Error
MSE	Mean Squared Error
RMSE	Root Mean Squared Error
MAPE	Mean Absolute Percentage Error
RMS	Root Mean Square
WT	Wavelet Transform
DWT	Discrete Wavelet Transform
IRT	Infrared Thermography
FFT	Fast Fourier Transform
DFT	Discrete Fourier Transform
NRAE	Noise Reduction Autoencoder
IF-GBDT	Improved Independent Forest–Gradient Boosting Decision Tree
OMT	Optimal Maintenance Timing
ER-MS	Evidential Reasoning with Maintenance–Storage impact
WPorNet	Weight Prototypical Network
GAF	Gramian Angular Field
DT	Digital Twin
MRF	Markov Random Field
MST-GNN	Multivariate Spatial-Temporal Graph Neural Network
MZI	Mach–Zehnder Interferometer
ANN	Artificial Neural Network
AFTC	Active Fault-Tolerant Control
DNN	Double Neural Networks
IFITSMC	Improved Fast Integral Terminal Sliding Mode Control
MGCN-TMIF	Modified Graph Convolution Network–Trusted Multi-Source Information Fusion
TS-HGNN	Time-Shifting based Hypergraph Neural Network

Received 2025-12-19; Accepted 2026-08-18; Available online 2026-08-25

ResNet	Residual Network
SCI-BiGRU	Spatial-Channel-Information Bidirectional Gated Recurrent Unit
FRACAS	Failure Report Analysis and Corrective Action System
RA	Reliability Analysis
CES	Complex Electromechanical Systems
EMS	Electromechanical System
IMFD	Induction Motor Fault Diagnosis
SVM	Support Vector Machine
RF	Random Forest
KNN	K-Nearest Neighbors
CNN	Convolutional Neural Network
RNN	Recurrent Neural Network
RPM	Revolutions Per Minute
CO_2	Carbon Dioxide
M	Number of samples / individuals in OPS population / Total number of samples
Q^{n}	n-dimensional feature space
W_l	Frequency coefficient at index l
z_s	Feature vector at time instance s
$\hat{Z}$	Reconstructed time-series sequence from LSTM-AE
ρ	Activation function (non-linearity in DC layers, e.g., ReLU)
$*$	Convolution operator
GPU	Graphics Processing Unit
lb	Lower bound of design variables in OPS
ub	Upper bound of design variables in OPS
$maxiter$	Maximum number of iterations in OPS
r	Random number in [0,1] for stochastic decision in OPS
h_1, h_2	Random scaling coefficients in OPS attack phase
w_{best}	Best current solution in OPS
$U^s_{chase\,1,j}$	Orca speed vector update during first chase phase at stage s
$U^s_{chase\,2,j}$	Orca speed vector update during second chase phase at stage s
$U^s_{attack\,1,j}$	Orca speed vector update during first attack phase at stage s
$U^s_{attack\,2,j}$	Orca speed vector update during second attack phase at stage s
$U^s_{attack,j}$	Final updated speed vector for j-th orca at stage s
$w^s_{chase\,1,j}$	j-th orca's updated position during first chase phase at stage s
$w^s_{chase\,2,j}$	j-th orca's updated position during second chase phase at stage s
$w^s_{chase\,3,j}$	j-th orca's updated position during third chase phase at stage s
$w^s_{attack,j}$	j-th orca's updated position after attack phase at stage s
$w^s_{first}, w^s_{second}, w^s_{third}, w^s_{four}$	Positions of randomly selected orcas for calculating attack updates
i_1, i_2, i_3	Indices of three randomly selected orcas for encircling strategy
a, b, d	Random numbers in [0,1] used in OPS equations
s	Stage index in OPS
v	Velocity factor in OPS encircling phase
$G(y)$	High-pass filter derived from selected mother wavelet
$G(-y)$	Low-pass filter capturing general trend of signal
$H(y)$	Complementary y-transform of high-pass filter
$w(s)$	Original time-domain signal
$(e * h)(w)$	Convolution output of input signal e(v) and kernel h(w-v)

1. INTRODUCTION

The modern industrial systems, along with manufacturing, power production, transportation, and automation, have electromechanical equipment as the operational backbone. These systems are becoming more complex and integrated; therefore, the probability of having unexpected failures and their effects in such systems increases rapidly, and crashes may result in costly downtimes, safety risks, and decreased productivity [1]. Conventional diagnostic approaches based mostly on manual inspection, approaching maintenance schedules, and fault detection based on rules are no longer enough to sustain the high efficiency of real-time industrial workplaces [2]. These traditional approaches are inelastic; they have problems with multi-source heterogeneous data and cannot be useful in detecting subtler or novel degradation patterns [3]. The intelligent diagnostic systems have now been introduced as a revolutionary solution due to the advent of sensing, data analytics technologies, and intelligent computing [4]. A Driven Intelligent Diagnostic System was an automatic method of detecting, classifying, and anticipating faults in the electromechanical equipment using machine learning, deep neural networks, and data-driven reasoning [5]. The system could combine multi-modal sensor-based inputs like vibration, acoustic assistances, current signatures, and thermal data to develop a complete picture of equipment health [6]. Data-driven models acquire intricate correlations, which allow detecting anomalies early, making faults easy to locate, and making pre-emptive maintenance decisions.

In addition, the system manages to self-learn to keep up with changing operating conditions, increasing its fault tolerance and diagnostic reliability [7]. Its predictive features enable organizations to shift from reactive or time-based strategies toward condition-based and forward-looking asset management approaches [8]. An Intelligent Diagnostic System that was driven would eventually not only upgrade equipment performance and upkeep continuity, but also lower maintenance expenses, mitigate hazards, and augment endurance in a wide range of electromagnetic uses [9]. Conventionally used diagnostic tools of the electromechanical equipment depend on the physical searches, threshold-based measurements, and rule-based expert systems that can frequently overlook the latent fault patterns and are not flexible enough [10]. Tools based on ML, like SVM, RF, and KNN, are better at identifying patterns, and tools based on DL, like CNN and RNN, are capable of allowing feature extraction and fault recognition with high accuracy.

The traditional, ML, and DL methods of diagnosis have constraints such as reliance on large labeled data, sensitivity to noise, non-stationary operating conditions, and high computational costs. Traditional methods are not flexible; the features of ML models must be created manually, and the features of DL models are black boxes, making them less interpretable. Such obstacles prevent real-time deployment, scalability, and reliability of complicated electromechanical systems. The aim was to develop a deep learning–driven intelligent diagnostic system for electromechanical equipment failures using a novel framework called OPS-DC-LSTM-AE, enhancing fault detection accuracy, adaptive learning, and reliable performance under complex operating conditions.

1.1 Key Contribution of the Research

- Data Collection: The Electromechanical Fault Dataset was obtained from Kaggle, which provides multivariate vibration, current, and acoustic signals under diverse operating conditions, labeled with fault types, enabling robust fault diagnosis research.
- Data Pre-processing: Applied WT for adaptive noise reduction, enhancing signal quality while preserving relevant fault characteristics across different operating conditions for accurate diagnostic modeling.
- Feature Extraction: Extracted temporal and frequency-domain features using FFT, including RMS, kurtosis, skewness, and peak amplitudes, capturing signal patterns critical for fault identification.
- Proposed Method: Implemented OPS-DC-LSTM-AE integrating Orca Predation Search optimization, Convolutional layers, LSTM, and AutoEncoder for intelligent, adaptive diagnosis of single and compound electromechanical faults.

2. RELATED WORKS

Table 1 shows the Overview of recent deep learning-driven electromechanical equipment fault diagnosis research.

Table 1. Advanced electromechanical equipment fault diagnosis and prediction related works summary

Ref. No.	Aim	Results	Advantages	Disadvantages
[11]	Developed a multi-branch ResNet combining three-phase and single-phase current analysis for IMFD.	DL and adaptive feature extraction achieved better diagnostic accuracy and reliability than Traditional ML.	Improved diagnostic accuracy and reliability.	High computational complexity.
[12]	Investigated combined mechanical and electrical fault diagnosis using SVM with vibration and current signals.	Signal fusion improved precision, and Continuous WT features performed better than time-domain features.	Improved precision through signal fusion.	Reduced performance during ramp-up time conditions.
[13]	Developed a Knowledge Graph-based intelligent inquiry system for metro electromechanical fault analysis.	Cypher querying and Naive Bayes Classification improved fault-handling accuracy and resource efficiency.	Accurate fault analysis and efficient resource utilization.	Dependence on semi-structured fault data.
[14]	Proposed a PdM-CNN model for automatic fault classification in rotating equipment using a single vibration sensor.	The model achieved accuracies of 99.58% and 97.3% on two public datasets.	High fault classification accuracy and reduced sensor acquisition cost.	Validation limited to controlled operating conditions.
[15]	Proposed the SCRLSTM model combining CNN, residual LSTM, and LSTM for anomaly detection in mechanical equipment.	The SCRLSTM model achieved better performance than other supervised learning models under various conditions.	Improved anomaly detection accuracy and feature extraction.	Increased model complexity.
[16]	Evaluated the reliability prediction of EMS using operational behaviour analysis.	The proposed method effectively predicted fault sequences and propagation probabilities.	Accurate fault sequence prediction.	Validation limited to single datasets.
[17]	Developed a sparse autoencoder-based multi-head	The method achieved satisfactory performance in both novelty detection and fault	Detects both known and unknown defects, reduced	Requires large monitoring datasets

	DNN for fault diagnosis and novelty detection.	diagnosis, outperforming existing methods.	computational burden, improved diagnostic performance.	for effective training.
[18]	Build an intelligent maintenance system using structured data cleaning and an IF-GBDT for low-label datasets.	Enhances classification accuracy, adaptability, and concurrency for small labeled data.	Effective with limited labels, robust preprocessing, and scalable.	Requires careful semi-supervised tuning; may struggle with high-dimensional noise.
[19]	Develop an OMT model using ER-MS for complex electromechanical equipment.	Improved reliability, transparency, and sensitivity analysis for INS systems.	Handles uncertainty well; accounts for historical maintenance effects.	Computational complexity requires extensive historical data.
[20]	An improved WPorNet using GAF for rolling bearing fault diagnosis.	Achieves higher accuracy and robustness than traditional prototypical networks.	Effective for few-shot learning; strong noise resistance, uses 2D signal encoding.	Image conversion increases computation and requires careful weight calibration.
[21]	Develop an interactive DT visualization framework for large electromechanical equipment.	Offline pre-rasterization + cloud fusion rendering enables fast rendering of complex models.	High rendering speed; supports design, production, and maintenance.	High system implementation cost; requires cloud resources.
[22]	Propose a fault prediction model using MRF and MST-GNN.	Effective long- and short-term prediction using spatial–temporal correlations.	Captures global and local relations; strong prediction accuracy.	Structure was computationally heavy; the graph design complexity.
[23]	Design vibration detection using MZI + ML	Achieved 98.5% accuracy in motor vibration frequency detection.	High precision; strong signal sensitivity; effective noise filtering.	Optical hardware was fragile and sensitive to environmental conditions.
[24]	Develop early multi-fault detection using IRT and an ANN classifier.	High recall and F1-score ensure reliable diagnosis.	Non-contact sensing; efficient early fault detection.	Sensitive to ambient temperature; limited for deep internal faults.
[25]	Implement AFTC using DNNs and IFITSMC for EMAs.	Superior fault sensitivity, reduced false alarms, enhanced tracking performance.	High robustness; strong real-time control; reliable detection.	Requires real-time tuning; increased controller complexity.
[26]	Integrate multisource signals with a graph-guided collaborative CNN and graph reasoning fusion to improve accuracy.	Outperforms 7 state-of-the-art methods, especially in noisy environments.	Excellent noise robustness; integrates multisource signals effectively.	High computational demand; requires multiple synchronized sensors.
[27]	Develop MGCN-TMIF using the Dirichlet distribution.	Achieves the highest classification accuracy with strong noise robustness.	Reliable multi-signal fusion; robust under uncertainty.	Complex fusion mechanism; high training cost.
[28]	TS-HGNN for fault type classification from current signals.	Effectively removes power-line interference and outperforms existing models.	Captures higher-order relationships; highly robust and accurate.	Hypergraph construction complexity requires high computing resources.
[29]	To develop a Dynamic Weight-Based Adaptive Data Fusion Filtering Algorithm combining an Extended Kalman Filter and wavelet denoising for accurate electromechanical condition monitoring.	Achieves 35.2% and 28.7% RMSE reduction, 41.5% and 34.3% MAE reduction compared to Kalman Filter and Particle Filter baselines.	Provides superior real-time reliability using variance-based stability metrics, adaptive weighting, and enhanced fault feature extraction for early industrial fault detection.	Slightly increased runtime relative to the standard Kalman Filter due to adaptive weighting and wavelet denoising, though still operationally acceptable.

[30]	Develop a fault prediction model for electromechanical actuators using SCI-BiGRU.	The SCI-BiGRU model accurately predicts multiple fault modes on the dataset reliably.	Provides high-precision early fault prediction, a unified multi-fault framework, robust temporal prediction, and effective feature extraction.	Requires high-quality signals, involves multi-stage computation, is dependent on temporal accuracy, and has limited dataset generalization.

2.1. Problem Statement

The multi-branch ResNet[11] model does not need any special datasets and has difficulty when the fault types are rare during extreme load changes. The hybrid mechanical-electrical diagnosis of SVM [12] will have poorer performance in ramp-up speed conditions and will rely heavily on high-quality features of CWT. It was inherent in the failure propagation probability model [16] that only with proper modeling of interdependency and system-specific configurations should it be generalized to other complex electromechanical systems without larger recalibration of the model. To address these shortcomings, a Deep Learning-based intelligent diagnostic model based on the OPS-DC-LSTM-AE framework that allows optimal feature extraction, adaptive learning, and extremely applicable electromechanical equipment fault detection.

3. METHODOLOGY

Electromechanical equipment data, including vibration, current, and acoustic signals, were collected under diverse operating conditions and labeled by fault types. Signals were pre-processed using WT for adaptive noise reduction, ensuring cleaner and more informative data. FFT was applied to extract temporal and frequency-domain features, capturing critical signal patterns. The proposed OPS-DC-LSTM-AE framework integrates optimized Convolutional, LSTM, and AutoEncoder layers for intelligent diagnosis of single and compound faults. Figure 1 shows the overall flow of methodologies

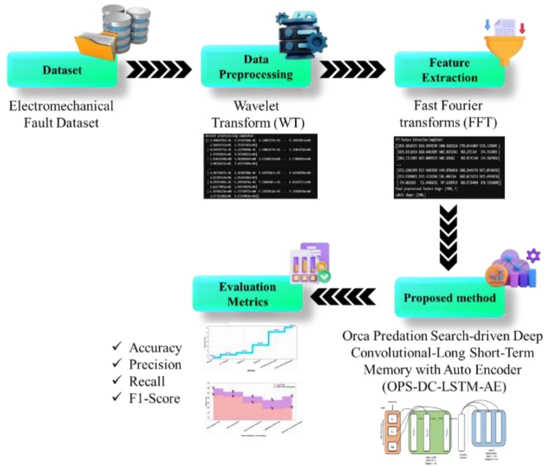

Fig. 1. Overall flow for electromechanical equipment failures

3.1. Data Collection

The Electromechanical Fault Dataset, which was collected from Kaggle [31], offers 2,300 multivariate samples representing realistic industrial machine behaviour under varying loads and speeds. It combines vibration, current, and acoustic sensor data with engineered time-domain (RMS, kurtosis, skewness) and frequency-domain (FFT mean, peak amplitude) features. Operational conditions like load percentage and RPM enrich state variability. Each instance is labeled with a fault_type, including normal, bearing fault, imbalance, and misalignment, supporting robust fault diagnosis research. The Dataset was partitioned using a 70% training, 15% validation, and 15% testing split to ensure balanced model training, hyperparameter tuning, and unbiased performance evaluation.

3.2. Data Pre-processing using WT for removing noise and decomposing sensor signals into multiple frequency bands, ensuring clean, detailed inputs for accurate fault diagnosis

WT-based data pre-processing decomposes non-stationary electromechanical signals into multi-resolution time–frequency components, enabling effective noise suppression, transient feature enhancement, and robust input preparation for the intelligent diagnostic system [32]. The multi-resolution decomposition of the raw acoustic signal $G(y)$ using the DWT. At each stage of decomposition, two digital filters, $G(y)$ and $G(-y)$, along with two down-samplers, are employed.$G(y^{-1})$, derived from the selected mother wavelet, acts as a high-pass filter to retain transient and high-frequency components indicative of leak signatures, while its mirror counterpart $G(-y^{-1})$ functions as a low-pass filter to capture the signal's general trend. The following was a representation of the connection between WTs and a filter$G$, or low pass, in equation (1).

$$G(y)G(y^{-1})+G(-y)G(-y^{-1})=1 \quad (1)$$

Where$H(y)$ stands for the filters $G(-y^{-1})$-transform. This is the expression for the complementary y-transform of the high-pass filter in equation (2). Figure 2 shows the WT denoises signals and preserves essential features for analysis.

$$H(y)=yG(-y^{-1}) \quad (2)$$

```
Wavelet preprocessing completed!
[[-5.49010783e-01 -3.47367560e-01  1.38815759e-01 ...  8.10323663e+00
   2.56656723e+01  1.79397247e+03]
 [-8.64939772e-01 -2.22299050e-01  3.20017879e-01 ...  9.36467818e+00
   2.97983013e+01  9.94760597e+02]
 [ 1.42616540e+00  1.48203014e+00  1.41336838e+00 ...  9.37004056e+00
   3.00286611e+01  9.96355304e+02]
 ...
 [-3.88774427e-01  6.20302700e-01  9.94379163e-01 ...  8.46550588e+00
   2.83385515e+01  1.49269201e+03]
 [-8.69591905e-01 -1.28954976e-02  5.58968901e-01 ...  8.85617511e+00
   2.82174051e+01  1.49470594e+03]
 [-1.43584124e+00 -1.53720737e+00 -7.29272028e-01 ...  9.25820958e+00
   2.97783201e+01  6.97250456e+02]]
```

Fig. 2. Wavelet-based pre-processing framework enhancing raw signals for diagnostic reliability

3.3. Feature Extraction using FFT is used for converting time-domain signals into frequency-domain features, helping identify dominant spectral patterns related to electromechanical faults

FFT converts raw electromechanical vibration or current signals into frequency-domain features, enabling the Driven Intelligent Diagnostic System to identify fault-specific spectral patterns for accurate failure detection [32]. The process of breaking down a function or signal over time into a component of frequency was known as the FFT. Condition-based maintenance leverages such analysis to predict and prevent potential failures, thereby enhancing system reliability. The perception of the Fourier transform was essential for sensor-based data processing, speech and communication, signal processing, and many other fields. Equation (3) describes the FFT mathematical form.

$$W(\zeta) = \int_{-\infty}^{\infty} w(s)\, f^{-2\pi j\zeta s} ds \qquad (3)$$

Here, $W(\zeta) \in D$ as Lebesgue integrals, and ζindicates the frequency. For practical use, FFT can be implemented quickly$\int_{-\infty}^{\infty} w(s)$. The DFT was calculated by FFT, which yields the same outcome as evaluating the DFT directly. The primary distinction of $f^{-2\pi j\zeta s}$ is that it was significantly quicker and ds less precise. Equation (4) represents the DFT mathematical form.

$$W_l = \sum_{m=0}^{M-1} w_m f^{-\frac{j2\pi lm}{M}}, (l = 0,..,M-1) \qquad (4)$$

The $W_l$was used to translate, and$\sum_{m=0}^{M-1}$ evaluate the spinning machine's data into the $w_m f^{-\frac{j2\pi lm}{M}}$frequencycoefficient at index $(l = 0$ plane from several experiments, $M-1$total samples. Figure 3 displays the FFT extracts dominant frequency patterns enabling accurate fault classification.

frequency-domain features, time-domain statistical features such as Root Mean Square (RMS), kurtosis, and skewness were directly computed from the raw sensor signals using fixed-length sliding windows. These features capture signal energy, impulsiveness, and distribution characteristics that are highly sensitive to mechanical faults. After extracting both time-domain and frequency-domain features, a sliding window-based sequence construction method was applied. Consecutive feature vectors were arranged chronologically to form time-ordered sequences, which were then fed into the LSTM network. This approach enables the model to capture the temporal evolution of spectral and statistical characteristics, thereby improving fault detection accuracy

3.4. DC used for extracting localized spatial features from sensor data, capturing subtle fault signatures through hierarchical convolutional filtering

DC networks enable a driven intelligent diagnostic system for electromechanical equipment failures by
.

```
FFT Feature Extraction Completed!
[[1829.20186353 1816.50591396 1800.56962626 1783.04148067 1776.1298849 ]
 [1035.82118524 1020.84013895 1002.45732963  982.2351549   974.3563059 ]
 [1042.73133095 1025.00093579 1002.824262    982.49742349  974.58474011]
 ...
 [1532.62061999 1517.96053699 1499.47084018 1480.29496742 1473.09544591]
 [1533.91890031 1519.31192364 1501.4097364  1482.66158218 1475.49920716]
 [ 734.6022614   722.94861232  707.11459515  685.57784034  676.72910206]]
Final preprocessed feature shape: (2300, 5)
Labels shape: (2300,)
```

Fig. 3. FFT-driven feature extraction converts signals into informative frequency components

automatically extracting multi-level spatiotemporal features from raw sensor signals. Their hierarchical learning structure enhances fault pattern recognition, improves diagnostic robustness, and supports real-time failure prediction, ensuring higher reliability and stability in complex industrial environments. DC was a family of neural networks with biological inspiration that solves equation (5) by subjecting W to several simple non-linearities and convolutional filters. The architecture of a DC was hierarchical. From the input signal w, each layer w_i, the following is calculated in equation (5).

$$w_i = \rho X_i w_{i-1} \quad (5)$$

ρ is a non-linearity, while X_i is a linear operator. Usually, ρ is a rectifier w_{i-1} is a convolution in a DC. The operator w_i is more easily conceptualized as a stack of convolutional filtering algorithms. The $i-th$ layer output at position v for feature map l_i. Here, w_{i-1} is the previous layer's feature, W_{i,l_i} is the convolutional kernel, $*$ denotes convolution, $\sum_l \left(w_{i-1}(.,l) * W_{i,l_i}(.,l)(v)\right)$aggregates across input channels, and ρ is the activation function, combining features into the next layer representation. Thus, each layer may be expressed as a sum of the convolutions of the one before it, and the layers are filter maps in equation (6).

$$w_i(v,l_i) = \rho(\sum_l \left(w_{i-1}(.,l) * W_{i,l_i}(.,l)(v)\right) \quad (6)$$

Where, $w_i(v,l_i)$ is the output feature map at layer i, position v, channel l.$,l$. $w_{i-1}(.,l)$ is the input map, $W_{i,l_i}(.,l)$ the convolution kernel, summed over input channels l and positions u, then activated by ρ denotes convolution. The discrete convolution operator in this case is $\sum_{v=-\infty}^{\infty}$, which represents the discrete convolution of two sequences e and h. Here, $e(v)$ is the input signal, $h(w-v)$ is the kernel or filter shifted by w, and the summation aggregates contributions from all positions v. Convolution combines the signals to produce the output sequence$(e*h)(w)$ in equation (7).

$$(e*h)(w) = \sum_{v=-\infty}^{\infty} e(v)h(w-v) \quad (7)$$

A DC defines an extremely non-convex optimization problem. Therefore, stochastic gradient descent is usually used to learn the weightsX_i, with gradients being computed using the backpropagation process.

3.5. LSTM-AE used for learning temporal dependencies and compressing features into latent representations, improving fault detection accuracy in sequential sensor data

LSTM-AE enhances driven intelligent diagnostic systems for electromechanical equipment failures by learning compressed representations and capturing long-term temporal dependencies in sensor data [33]. Its combined structure improves fault feature extraction, anomaly detection accuracy, and robustness, enabling early prediction of complex, nonlinear failure patterns in industrial equipment. LSTM-AE integrates AE and LSTM networks, leveraging their strengths. The encoder converts high-dimensional input sequences into fixed-size vectors, preserving temporal dependencies via LSTM memory cells. It progressively reduces dimensionality until reaching the latent space. The LSTM decoder reconstructs input sequences from these compressed representations.

Step1: Input Sequence Data

$[Z_1, Z_2, Z_3, \ldots., Z_n]$is the time sequence that makes up the original dataset. $z_s \in Q^n$ denotes an n-features input at time instance$s$, and each sequence W with a fixed time window data $[z_1, z_2, z_3, \ldots., z_s]$ is generated. After that, it is once more transformed into a $2d$-dimensional array that represents timesteps and samples. For instance, a $2d$ array is created from a sequence of the CO_2 data, where every dimension represents a list of samples.

Step2: LSTM Encoder

The LSTM encoder's primary function is to convert features into a batch of time-based feature sequences by functioning as a sequence folding layer. It is comparable to independently performing convolution operations on feature sequence time steps. The most important aspects of the input sequence were the details of the encoder's interaction with the training set of LSTM unit cells. Ten samples were taken at ten-time steps in each W_j time series. For instance, to unroll the input dataset according to time steps, the number of income is desired as a $2d$ vector, with 10 time steps in one dimension and features in another, resulting in a vector of 10×1. $Layer$ 1 is created by the encoder and comprises a $10-cell$ LSTM network. A sample is processed successively by each cell. The second LSTM receives the sample result from the first LSTM and determines whether to retain or discard the prior sample. It transfers the data to the third LSTM and stores it in long-term memory if it retains it. All pertinent samples processed by the preceding nine LSTM cells are output by the tenth LSTM, which transforms them into encoded features. Figure 4 shows an intelligent diagnostic pipeline where ten sensor-derived feature vectors z_1, z_2, z_{10}form the input. These sequential features are fed into a multi-layer LSTM network that learns temporal patterns of electromechanical equipment behaviour. The final LSTM outputs pass through fully connected layers to generate the system's output: predicted fault classes or health-status indicators. This structure enables deep, time-dependent fault detection for electromechanical machinery.

The purpose of creating as many copies of the 1×16 vector as there are time steps, introduced a Repeat Vector as$Layer$ 2. As an illustration, since the model's time steps are 10 in size, $Layer$ 2.

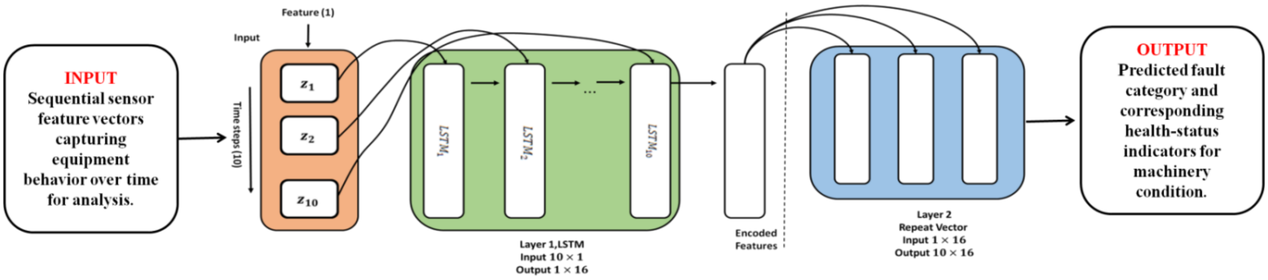

Fig. 4. LSTM architecture capturing temporal dependencies for robust fault diagnosis

generates 10 $copies$ of the encoded features as a $2d$ vector with dimensions of 10×16

Step3: Identification of Anomalies

An anomaly is an observation that deviates from the main data trend. A threshold is set to identify anomalies based on the extent. Using a dataset of normal CO_2 measurements, a threshold-based anomaly detection technique is applied. Reconstruction error rates for typical CO_2 data points are obtained. The highest reconstruction error is set as the threshold. The test dataset, containing all CO_2 ranges, is analyzed. If a CO_2 value's reconstruction error exceeds the threshold, it is classified as abnormal. As indicated by the blue dotted blocks, let's assume that there are five samples $[z_1, z_2, z_3, z_4, z]$that are composed of three time-series sequences of $[Z_1, Z_2, Z_3]$, each of which contains three samples on three distinct time steps, where $Z_1 \in [z_1, z_2, z_3]$, $Z_2 \in [z_2, z_3, z_4]$, and $Z_3 \in [z_3, z_4, z_5]$. These three time series of sequences are used as inputs by the model, which then creates outputs that correspond to each of the following sequences: $\hat{Z}_1 \in [\hat{z}_1, \hat{z}_2, \hat{z}_3], \hat{Z}_2 \in [\hat{z}_2, \hat{z}_3, \hat{z}_4]$, and$\hat{Z}_3 \in [\hat{z}_3, \hat{z}_4, \hat{z}_5]$.Each sample's reconstruction loss can be computed in equations (8) – (12).

$$z_1 = \frac{|1.1-1|}{1} = 0.1 \tag{8}$$

$$z_2 = \frac{|2.02-2|+|1.99-2|}{2} = 0.01 \tag{9}$$

$$z_3 = \frac{|3.01-3|+|2.99-3|+|3.01-3|}{3} = 0.01 \tag{10}$$

$$z_4 = \frac{|3.99-4|+|4.01-4|}{2} = 0.01 \tag{11}$$

$$z_5 = \frac{|5.02-5|}{1} = 0.02 \tag{12}$$

A threshold is established for the maximum reconstruction loss, and the value is 0.1. Any samples in which the reconstruction loss during testing exceeds 0.1 are now classified as anomalous.

3.6. OPS used for optimizing hyperparameters by simulating orca hunting behaviour, improving model efficiency, accuracy, and convergence speed

An OPS enhances a driven, intelligent diagnostic system for electromechanical equipment failures by optimizing deep learning model parameters through predator–prey-inspired exploration [34]. An OPS strengthens feature selection, accelerates convergence, and improves fault classification accuracy, enabling robust, adaptive, and reliable detection of complex equipment failures under dynamic industrial conditions. The OPS is a bio-inspired computational optimization technique that mimics orcas' hunting techniques. The goal is to solve challenging optimization issues by mimicking the sophisticated and well-coordinated hunting methods of orcas. The driving and encircling phases make up the algorithm's two separate phases. Important parameters such as the number of individuals(M), length(C), maximum instance, selection probability (o_1, o_2), lower bound (lb), and the upper limit $(ub)$of the design variables are established in the initial phase of OPA. The initial location of the orca group is determined at random within the given bounds. The orca with the greatest fitness value, referred to as the best current solutionw_{best}. Based $U^s_{chase\ \ 1,j}, U^s_{chase\ \ 2,j}$ are decision's probability. The decision made determines whether the orca will focus on exploitation or exploration. Orcas use sonar to adjust their position by recalculating it using the following equations (13) – (17).

$$U^s_{chase\ \ 1,j} = b\left(cw^s_{best} - E\left(aN^s + dw^s_j\right)\right) \tag{13}$$

$$U^s_{chase\ \ 2,j} = fw^s_{best} - w^s_j \tag{14}$$

$$N = \frac{\sum_{j=1}^{M} w^s_j}{M} \tag{15}$$

$$d = 1 - a \tag{16}$$

$$\begin{cases} w^s_{chase\ 1,j} = w^s_j + U^s_{chase\ 1,j} if rand > r \\ w^s_{chase\ 2,j} = w^s_j + U^s_{chase\ 2,j} if rand \le r \end{cases} \tag{17}$$

Where s is the quantity of stages, u^s is the speed of pursuit, N are orca group's standard position, w^s is the orca's location, b, a, and ddare are random integers between [0,1], $w^s_j + U^s_{chase\ 1,j}, w^s_j + U^s_{chase\ 2,j}$ is an arbitrary number, and s = 2, and r is a number among [0,1]. The orca encircles its victims in equations (18) and (19).

$$w^s_{chase\ 3,j} = w^s_{i\ 1,j} + v\left(w^s_{i\ 2j} - w^s_{i\ 3,j}\right) \tag{18}$$

$$v = 2(rand - 0.5)\frac{maxiter - s}{maxiter} \tag{19}$$

Where i_1, i_2,and$i_3$indicate three different orcas chosen at random so that$i_1 \neq i_2 \neq i_3$, and $maxiter - s$,$2(rand - 0.5)$represents the maximum number of iterations. After choosing the third pursuit strategy at time$s$, the $j - th$ whale's position is shown by$w^s_{chase\ 3,j}$. During the attack phase, the position is updated in the fourth phase. Orcas improve $w_{i\,1,j}^{s}$their posture to successfully attack prey at this stage. The $v(w_{i\,2j}^{s} - w_{i\,3,j}^{s})$location is revised in accordance with equations (20)–(22). Some orcas may reach the search zone's limits during the attack. The returns are lower than the limit (lb) beyond the limit.

$$u_{attack\ 1,j}^{s} = \frac{\left(w_{first}^{s}+w_{second}^{s}+w_{third}^{s}+w_{four}^{s}\right)}{4-w_{chase\ ,j}^{s}} \quad (20)$$

$$u_{attack\ 2,j}^{s} = \frac{\left(w_{chasej}^{s}+w_{chase\ 1,j}^{s}+w_{chase\ 2,j}^{s}\right)}{3-w_{j}^{s}} \quad (21)$$

$$u_{attack,j}^{s} = w_{chase,j}^{s} + h_1 u_{attack\ 1,j}^{s} + h_2 u_{attack\ 2,j}^{s} \quad (22)$$

Where $u_{attack\ 1,j}^{s}u_{attack\ 2,j}^{s}u_{attack,j}^{s}$denotes the $j-th$ orca's speed vector at time during their hunting phase s, $vu_{attack\ 2,j}^{s}$ depicts the $j-th$ orca's speed vector as it returns to the enclosure at times, w_{first}^{s}, w_{second}^{s}, w_{third}^{s}, andw_{four}^{s} indicate. During the chase phase, $w_{chase\ 1,j}^{s} + w_{chase\ 2,j}^{s} + w_{chase\ 2,j}^{s}$three orcas were selected at random from the entirety of M, guaranteeing $i_1 \neq i_2 \neq i_3$. $w_{attack,j}^{s}$ is the $j-th$ orca's location at time s after the attack phase, h_1 is a random value in the region $[0,2]$, and h_2 is a random number. The creation of an entire population is the fifth phase. The results of the pursuit and attack phases are used to adjust the orcas' locations. This phase preserves the determined ideal solution while guaranteeing population variety.

OPS optimizes the hyperparameters of the DC-LSTM-AE model by simulating orca hunting behaviour, enhancing feature selection, accelerating convergence, and improving fault classification accuracy. This bio-inspired approach ensures robust, adaptive, and reliable detection of both single and compound faults in electromechanical equipment under dynamic and noisy conditions. Standard methods are either computationally expensive, lack guided exploration, or can get trapped in local optima. OPS overcomes these limitations with predator–prey-inspired search, providing faster convergence, better hyperparameter optimization, and higher diagnostic accuracy.

3.7. An Optimized Deep Learning Hybrid Model (OPS-DC-LSTM-AE) for Electromechanical Failure Detection

The proposed OPS-DC-LSTM-AE model is a hybrid deep learning architecture designed for intelligent fault diagnosis of electromechanical equipment by integrating spatial feature extraction, temporal modeling, latent representation learning, and metaheuristic optimization. The Deep Convolutional (DC) module consists of stacked convolutional layers followed by Rectified Linear Unit (ReLU) activation and optional pooling layers. These layers perform hierarchical convolution operations to extract localized fault signatures from preprocessed FFT-based sensor inputs. The convolutional filters learn multi-scale spatial representations, while pooling reduces dimensional redundancy and enhances translational invariance. The extracted feature maps are reshaped into sequential inputs and fed into multi-layer LSTM networks. Each LSTM layer contains memory cells with input, forget, and output gates that regulate information flow, enabling the model to capture long-term temporal dependencies and fault evolution patterns. The encoder compresses these sequential features into a fixed-length latent vector, forming the Autoencoder bottleneck layer. The decoder reconstructs the original sequence, and reconstruction loss is computed for anomaly detection. To optimize network hyperparameters, the OPS algorithm iteratively updates learning rate, filter count, kernel size, and LSTM units, enhancing convergence stability, global search capability, and diagnostic accuracy. Algorithm 1 shows the procedure of OPS-DC-LSTM-AE. Table 2 shows the hyperparameters of OPS-DC-LSTM-AE.

Algorithm 1:OPS-DC-LSTM-AE

$Input$:
$RawelectromechanicalsignalsS\ (vibration, current, acoustic)$
$Loadpercentage, RPM, fault\_typelabels$
$WaveletfiltersG(y), G(y^{-1}), H(y)$
$FFTparameters\ (Msamples, frequencyindex\zeta)$
$DCparameters\ \{W\_(i, l\_i), \rho, layers\}$
$LSTM - AEparameters\ \{timestepsT, latentsize, cells\}$
$OPSparameters$:
$M\ (populationsize), C\ (dimensions)$,
$maxiter\ (maximumrepetitions), selectionprobabilitieso1, o2$,
$Boundslb, ub$
$Output$:
$Optimizeddiagnosticmodel \rightarrow Faultclasspredictionoranomalydetection$
$BEGIN$
$LoadElectromechanicalFaultDataset$:
2300 $samples\ containing\ multivariate\ signals$:
$S = \{vibration, current, acoustic\}$
$Extract\ operational\ metadata$:
$load\_percentage, RPM$

$Labels: fault\_type \in \{normal, bearing\_fault, imbalance, misalignment\}$
$ForeachsignalsinS:$
$PerformDWTmultiresolutiondecomposition:$
$UsefiltersG(y^{-1})\ (high - pass)\ andG(-y^{-1})\ (low - pass)$
$Validatefiltercondition:$
$G(y)G(y^{-1}) + G(-y)G(-y^{-1}) = 1$
$Computecomplementarytransform:$
$H(y) = yG(-y^{-1})$
$Obtain: approximation\ coefficients\ A\ and\ detail\ coefficients\ D$
$Removenoise, reconstructcleansignalsS\_clean$
$Foreachcleanedsignalw(s):$
$ComputeFFT:$
$W(\zeta) = \int w(s) * f\hat{}(-2\pi j\zeta s)\, ds$
$ComputeDFTforpracticalimplementation:$
$Forl = 0\ toM - 1:$
$W\_l = \Sigma\_\{m = 0\}\hat{}\{M - 1\}\ (w\_m * f\hat{}(-j\pi m/M))$
$Extractspectralfeatures:$
$meanamplitude, dominantfrequency, harmonicpeaks$
$InitializeDClayerswithkernelsW\_(i, l\_i)$
$Setw_0 = FFTfeaturemaps$
$Foreachlayeri:$
$Compute:$
$w\_i = \rho(X\_iw\_(i - 1))$
$Foreachpositionvandfeaturemapl\_i:$
$w\_i(v, l\_i) = \rho(\Sigma\_l\ (w\_(i - 1)(.,l) * W\_(i, l\_i)(.,l)(v)))$
$Computediscreteconvolution:$
$(e * h)(w) = \Sigma\_\{v = -\infty\ to\ \infty\}\ e(v)\ h(w - v)$
$OutputDCfeaturemapsF\_DC$
$Step\ 1: Construct\ Input\ Sequences$
$Convert\ data\ into\ sequences:$
$Z = [Z_1, Z_2, \ldots, Z\_n], eachZ\_s \in Q\hat{}n$
$FormT - lengthwindows:$
$W = [z_1, z_2, \ldots, z\_T]$
$Step\ 2: LSTMEncoder$
$Unrollsequencesinto\ 2Darray\ (T \times feature\_dim)$
$Passthrough\ 10 - cellLSTMnetwork$
$FinalLSTMcelloutputsencodedvectorEnc$
$RepeatVectorproducesTcopiesofEnc$
$Step\ 3: LSTMDecoder$
$Decodesequences \rightarrow reconstructedoutputs\hat{Z}$
$Step\ 4: Compute\ Reconstruction\ Loss\ per\ sample:$
$z_1 \ldots z_5\ computedas:$
$z\_k = average\ (|\hat{z} - z|)$
$Step\ 5: Thresholding$
$threshold = max(reconstruction\_loss\_normal)$
$Ifloss(test) > threshold \rightarrow classifyasanomaly$
$OutputLSTM - AEanomalyscores + EncodedfeaturesF\_LSTM$
$Initialize:$
$Randomly\ generate\ Morca\ positions\ w\_jwithin\ [lb, ub]$
$Evaluatefitnessforeachw\_jusingmodelvalidationaccuracy$
$Identifybestsolutionw\_best$
$Fors = 1\ to\ maxiter:$
$Computegroupaverage:$
$N = (\Sigma\_\{j = 1\}\hat{}\{M\}\ w\_j)\ /\ M$
$Computed = 1 - a$
$Foreachorcaj:$
$Generaterand \in [0,1]$
$Ifrand > r:$
$U\_(chase1, j)\hat{}s = b\ (cw\_best - E(aN + dw\_j))$
$Else:$
$U\_(chase2, j)\hat{}s = fw\_best - w\_j$
$Update\ pursuit\ position:$
$Ifrand > r:$
$w\_(chase, j)\hat{}s = w\_j + U\_(chase1, j)\hat{}s$
$Else:$
$w\_(chase, j)\hat{}s = w\_j + U\_(chase2, j)\hat{}s$
$Selecti1 \neq i2 \neq i3\ randomly$

$v = 2(rand - 0.5) * (maxiter - s)/maxiter$
$w\_(chase3, j)\^s = w\_(i1, j)\^s + v\,(w\_(i2, j)\^s - w\_(i3, j)\^s)$
$Compute\ attack\ speeds$:
$u\_(attack1, j)\^s = (w\_first + w\_second + w\_third + w\_four)\,/\,(4 - w\_(chase, j))$
$u\_(attack2, j)\^s = (w\_(chase1, j) + w\_(chase2, j) + w\_(chase2, j))\,/\,(3 - w\_j)$
$Update$:
$w\_(attack, j)\^s = w\_(chase, j)\^s + h1\,u\_(attack1, j)\^s + h2\,u\_(attack2, j)\^s$
$Enforcebounds$:
$Ifw\_(attack, j)\^s < lb \rightarrow settolb$
$Ifw\_(attack, j)\^s > ub \rightarrow settoub$
$Updatew\_bestifimprovedfitnessfound$
$Outputoptimizedparameters\theta * = w\_best$
$CombineDC + LSTM - AE + OPSoptimizedparameters$:
$PredictfaulttypeORanomaly$
$Returndiagnosticdecision$
END

Table 2. Hyperparameters of OPS-DC-LSTM-AE

Component	Hyperparameter	Suggested Value / Range
Deep Convolution	num_layers	3
	kernel_sizes	[3, 3, 3]
	num_filters	[64, 32, 16]
	activation	ReLU
LSTM-AE	timesteps	10
	encoder_units	[32, 16]
	latent_dim	16
	decoder_units	same as encoder
	batch_size	32
	epochs	100 (final), 5–10 (for OPS fitness)
OPS	population_size (M)	20
	dimensions (C)	depends on the hyperparam vector size
	max_iterations (maxiter)	50
	selection_probabilities (o1, o2)	[0.5, 0.5]
	bounds (lb, ub)	depends on each hyperparameter
	Random factors (a, b, d, f, h1, h2)	a,b,d,f ∈ [0,1], h1 ∈ [0,2], h2 ∈ [-2.5,2.5]
	Convergence Criterion	Maximum Iterations = 100
	Fitness Function	Minimize Fitness Value (Best objective score per iteration)
	Stability Evaluation	Mean fitness ± 2 × Standard Deviation over 5 independent runs
	Search Strategy Balance	Early Exploration (Iterations 1–40), Transition Phase (41–70), Strong Exploitation (71–100)
OPS-DC-LSTM-AE (Full Hybrid Model)	Training Time	~60 minutes (100 epochs, including OPS runs)
	Memory Usage	~4 GB (GPU)

4. RESULT

The proposed OPS-DC-LSTM-AE model was implemented using Python-based deep learning frameworks and trained on a high-performance computing platform. Efficient and stable training was ensured through optimized batch processing, multiple training epochs, and adaptive learning-rate scheduling. Table 3 summarizes the hardware and software configuration used for training and evaluation.

The following metrics were used to evaluate the suggested approach and ascertain its efficacy: Accuracy, F1-score, Precision, Recall, MAE, MSE, RMSE, and MAPE. Additionally, a comparative analysis was carried out with other current methods, such as SSA-BiGRU-Attention [30], CPL [30], 2D-CNN [30], SFUDA [30], and ECAAE [30]. Both the DC-LSTM-AE and OPS-DC-LSTM-AE models are trained using the Electromechanical Fault Dataset to improve fault detection and diagnostic accuracy.

Table 3. Hardware and software configuration for electromechanical fault diagnosis training

Parameter	Configuration
Programming Language	Python
Hardware	NVIDIA RTX 3080 GPU, 32 GB RAM
Epochs	150
Batch Size	32
Learning Rate	0.001 (Adam)

Figure 5 mentions the convergence plot of the part of the proposed models' OPS optimization. The mean convergence curve shows a rapid reduction in fitness value during early iterations, followed by stable fine-tuning. The upper and lower variation lines indicate solution stability, demonstrating consistent performance and controlled exploration–exploitation balance.

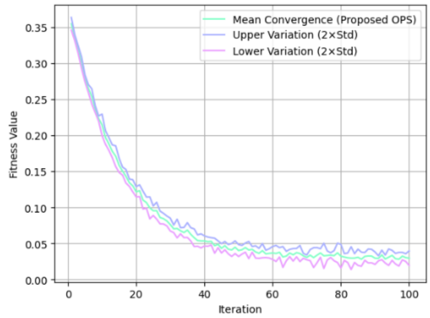

Fig. 5. Convergence behaviour of the proposed OPS algorithm

Figure 6 shows the trends of the performance of the OPS-DC-LSTM-AE-based Driven Intelligent Diagnostic System of Electromechanical Equipment Failures. The accuracy graph reveals that the accuracy of the training and validation improves with the number of epochs, indicating efficient feature extraction and time learning. The loss curve shows a consistent convergence; the training and validation loss continue to decrease, which means consistency of the reconstruction and identification of anomalies. The combination of curves justifies the strength, profitability, and predictability of the system.

The multimodal sensor behaviour recorded on vibration, current, and acoustic channels is visualised in the 3D scatter and is the core input space of the OPS-DC-LSTM-AE-based driven intelligent diagnostic system. This value might not be meaningful due to the nonlinear relation needed in deep temporal-spatial features, by indicating dense populations of operating states in a variety of loads and speeds. These various raw signals aid in the proper identification of the faults in the electromechanical equipment. Figure 7 illustrates clustered sensor measurements in the creation of nonlinear patterns in diagnostic learning.

The scatter-matrix shows pairwise associations and distributions among vibration, current, and acoustic signals, which are critically important in feature behaviour in OPS-DC-LSTM-AE-based fault diagnosis of electro-mechanical error detection. This visualization assists in establishing normality patterns as well as in determining possible correlation patterns, as well as data homogeneity across modalities. This characterization of statistics empowers the pre-processing step, allowing the deep hybrid model to acquire hearty temporal representations and maximize diagnostic reliability by the fault type. Figure 8 presents the related signal relationships in pairs, which prove statistical validation before the modelling.

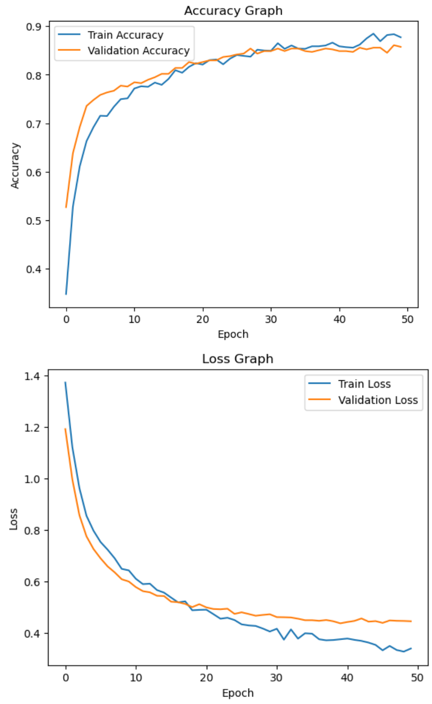

Fig. 6. Training and validation performance curves for model accuracy and loss

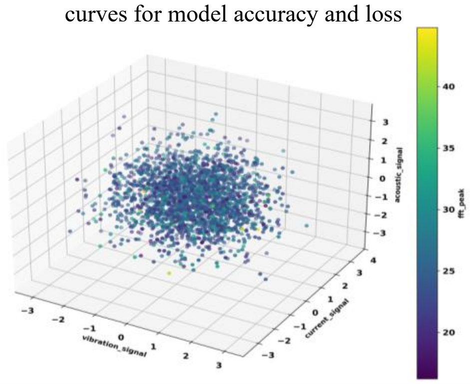

Fig. 7. 3D Multisensor scatter plot showing vibration, current, acoustic variations

The 3D hyperboloid surface reflects geometric designs like engineered kurtosis, skewness, and speed variations, and demonstrates the concept of nonlinear geometric transformations, which are applicable to the model of a diagnostic based on OPS-DC-LSTM-AE. This design makes a difference between the dynamic range and advancement of statistical descriptors at different operating speeds. The DL is effective in terms of feature landscapes because it can map higher-order signal features that would improve the ability of the system to detect failures in electromechanical equipment. Figure 9 presents the geometric change of statistical characteristics of machines in various working conditions.

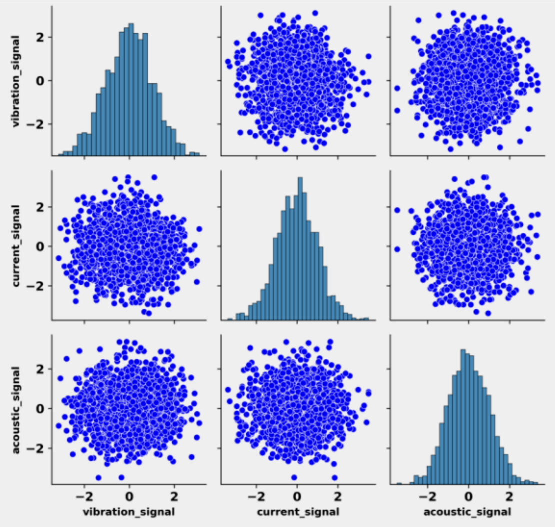

Fig. 8. Multimodal sensor scatter matrix with distributions and correlation insights

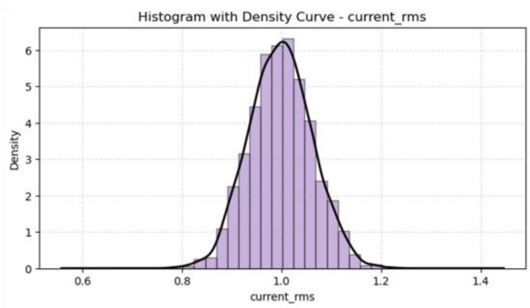

Fig. 9. Hyperboloid surface illustrating engineered feature behaviour across speed levels

The OPS-DC-LSTM-AE-informed diagnostic process demonstrates the statistical dependency among vibration and current RMS signals. This is a highly correlated behaviour that is played out in the base preprocessing to stabilize dynamic channels before dual-cascade LSTM encoding. The autoencoder part restores the synchronized temporal trends, and this allows detection of deviations due to mechanical degradation in time. The correlations offer a necessary baseline behaviour to be utilized in the anomaly scoring and condition-aware fault progression tracking. Figure 10 shows the vibration-current relationship distributions, indicating consistency in the operation of the baseline.

The correlation–clustering map illustrates feature relevance for the OPS-DC-LSTM-AE diagnostic pipeline. Low cross-correlations between FFT features and higher-order vibration statistics indicate complementary information sources. OPS preprocessing selects stable windows; DC-LSTM layers fuse spectral–statistical cues; and the autoencoder isolates nonlinear interdependencies. The dendrogram guides dimensionality reduction and enhances feature grouping, enabling more efficient latent-space learning and improving generalization across diverse electromechanical fault conditions. Figure 11 shows feature relationships and clustering structure aiding model preprocessing decisions.

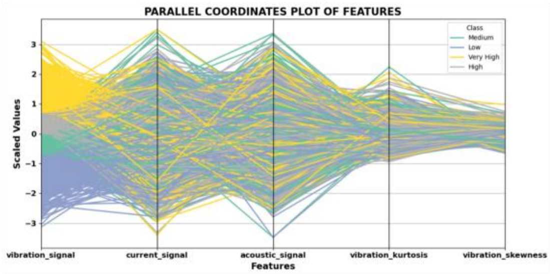

Fig. 10. Correlation scatter with marginal histograms for multimodal signal evaluation

The multimodal feature class-level separability at the key features in the OPS-DC-LSTM-AE diagnostic system is shown using parallel coordinates. An operating state is normalized by OPS, and temporal signatures are learnt by two layers of cascaded LSTMs due to vibration, current, acoustic, and spectral signatures. The AE condenses and regenerates these behaviours, and by this, the system is able to signal outliers. Discriminable trends on a visible basis through the classes indicate the use of feature discriminability in understanding strong real-time fault detection across electromechanical machines. Figure 12 shows the trends of features showing the separability of conditions of electromechanical systems.

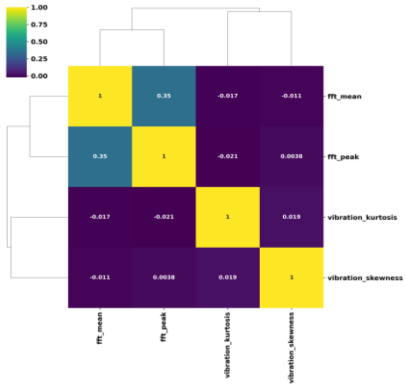

Fig. 11. Clustered feature-correlation heatmap guiding multimodal diagnostic feature selection

The OPS-DC-LSTM-AE model exhibits superior reliability and generalization compared to the baseline DC-LSTM-AE across all evaluated metrics. The cross-validation score improved from 85.2% to 87.8%, and test set performance increased from 84.5% to 86.4%. Failure prediction consistency rose from 82.0% to 84.5%, while adaptability to new faults significantly improved from 79.5% to 83.1%. Additionally, robustness to operational changes increased from 80.0% to 84.6%. These results demonstrate that the proposed model offers enhanced stability, adaptability, and predictive consistency for electromechanical equipment diagnostics. Table 4 and Figure 13 display the comparative evaluation of model performance across diverse test scenarios.

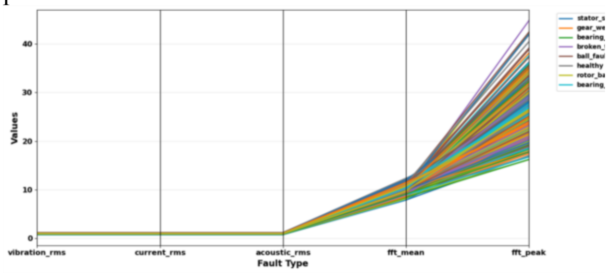

Fig. 12. Parallel-coordinates visualization comparing multimodal features across fault classes

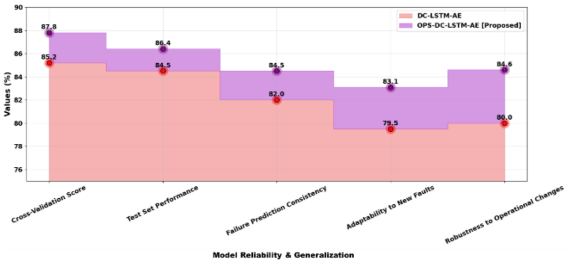

Fig. 13. Electromechanical equipment diagnostics performance across reliability metrics

Table 4. Reliability and generalization metrics for electromechanical equipment diagnostics

Model Reliability & Generalization	DC-LSTM-AE (%)	OPS-DC-LSTM-AE [Proposed] (%)
Cross-Validation Score	85.2	87.8
Test Set Performance	84.5	86.4
Failure Prediction Consistency	82.0	84.5
Adaptability to New Faults	79.5	83.1
Robustness to Operational Changes	80.0	84.6

4.1. Performance Evaluation

- Accuracy: This is a measure that shows how accurate the diagnostic system is by determining the percentage of correctly identified failures and normal operations relative to the total number of inspections performed on the electromechanical equipment.
- Precision: Measures the accuracy of identified failures, where many failures are correctly identified out of all those that were identified through such equipment monitoring as failures.
- Recall: Measures the capability of the system to identify real failures, where the ratio of truly captured failures to the number of real failures of electromechanical equipment in the process of diagnostics.
- F1-Score: The balanced score gives a measure of the diagnostic system in general terms of correct error detection, both false and true electromechanical equipment failures, as well as false positives and negatives.
- MAE: Measures the average magnitude of prediction errors, indicating overall accuracy in diagnosing electromechanical faults without considering error direction, reflecting system reliability.
- MSE: Quantifies the average squared differences between predicted and actual fault signals, emphasizing larger deviations, highlighting robustness of the diagnostic system.
- RMSE: Represents the square root of MSE, providing error in original units, indicating sensitivity to large fault prediction deviations in electromechanical equipment.
- MAPE: Expresses prediction errors as percentages, showing relative diagnostic accuracy, allowing comparison across varying fault magnitudes and operating conditions.

The evaluation of the diagnostic system for electromechanical equipment failures demonstrates that the proposed OPS-DC-LSTM-AE method significantly outperforms the conventional DC-LSTM-AE. The MAE is reduced from 6.42 to 5.33, MSE from 4.95 to 2.67, RMSE from 2.22 to 1.24, and MAPE from 7.18 to 5.02, confirming enhanced prediction accuracy and robustness. These improvements reflect the effectiveness of OPS-based hyperparameter optimization combined with the DC-LSTM-AE architecture, establishing a highly reliable and precise intelligent diagnostic framework for electromechanical fault detection. Table 5 shows improved error performance using the proposed model for electromechanical equipment failure

Table 5. Error metrics comparison in diagnostic system for electromechanical equipment failures

Metric	DC-LSTM-AE	OPS-DC-LSTM-AE (Proposed)
MAE	6.42	**5.33**
MSE	4.95	**2.67**
RMSE	2.22	**1.24**
MAPE (%)	7.18	**5.02**

The comparative evaluation of diagnostic models shows progressive improvements across methods. CPL achieves 91.55%, 2D-CNN reaches 92.14%, and SFUDA attains 92.55%, reflecting modest gains in feature extraction and domain alignment. ECAAE further improves performance to 94.26%, while SSA-BiGRU-Attention significantly boosts accuracy to 97.14% through sequential feature learning. The proposed OPS-DC-LSTM-AE model delivers the highest accuracy of 98.12%, demonstrating its superior capability in capturing complex electromechanical equipment fault patterns for a highly reliable intelligent diagnostic system. Table 6 and Figure 14 show the performance comparison showing accuracy improvements across multiple intelligent diagnostic models.

Table 6. Comparative accuracy results of diagnostic methods for electromechanical equipment failures

Methods	Accuracy (%)
CPL [30]	91.55
2D - CNN [30]	92.14
SFUDA [30]	92.55
ECAAE [30]	94.26
SSA-BiGRU-Attention [30]	97.14
OPS-DC-LSTM-AE [Proposed]	98.12

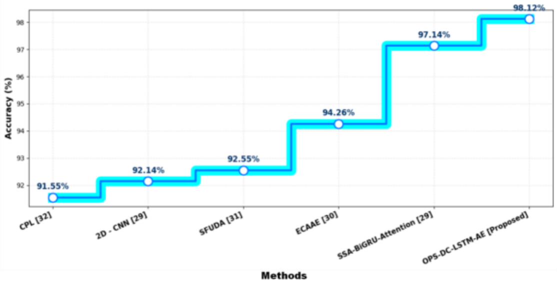

Fig. 14. Accuracy comparison of proposed and existing diagnostic approaches

The performance comparison highlights the effectiveness of advanced deep learning models for electromechanical equipment fault diagnosis. The SSA-BiGRU-Attention model achieves 96.27% precision, 95.83% recall, and 96.04% F1-score, demonstrating strong sequential feature extraction. However, the proposed OPS-DC-LSTM-AE outperforms it with 98.06% precision, 97.04% recall, and 98.11% F1-score, indicating superior capability in capturing complex fault patterns. These results confirm the robustness and reliability of the proposed Driven Intelligent Diagnostic System for electromechanical equipment failures. Table 7 displays the performance values comparing the proposed system with the existing diagnostic approach.

Table 7. Performance comparison of existing and proposed models for equipment diagnostics

Methods	Precision (%)	Recall (%)	F1-Score (%)
SSA-BiGRU-Attention [30]	96.27	95.83	96.04
OPS-DC-LSTM-AE [Proposed]	98.06	97.04	98.11

The suggested OPS-DC-LSTM-AE framework, CPL [30], 2D-CNN [30], SFUDA [30], ECAAE [30], LSTM, CNN and SSA-BiGRU-Attention [30] were trained and evaluated for electromechanical fault detection using the Electromechanical Fault Dataset. Table 8 displays a comparison of all models' classification performance indicators, such as accuracy, precision, recall, and F1-score.

Table 8. Comparative assessment of electromechanical fault diagnosis performance across various models on the Electromechanical Fault Dataset

Methods	Accuracy (%)	Precision (%)	Recall (%)	F1-Score (%)
CPL	89.45	88.92	87.60	88.20
2D-CNN	91.80	91.25	90.10	90.60
SFUDA	92.75	92.10	91.40	91.75
ECAAE	94.20	93.85	93.10	93.45
SSA-BiGRU-Attention	96.30	96.05	95.20	95.60
LSTM	93.10	92.60	91.80	92.20
CNN	90.40	89.85	88.70	89.20
OPS-DC-LSTM-AE [Proposed]	98.12	98.06	97.04	98.11

The suggested OPS-DC-LSTM-AE architecture was found to perform better than the current approaches on all evaluation measures. The combined DC-LSTM-AE architecture improves accuracy, precision, recall, and F1-score by extracting temporal and frequency-domain data effectively, optimizing hyperparameter tuning with OPS, and learning resilient fault representations. The findings of the experiments confirm better diagnostic performance for intelligent industrial equipment monitoring applications, increased reliability in fault categorization, and improved detection of both single and compound electromechanical defects.

To evaluate the robustness and generalization capability of the proposed OPS-DC-LSTM-AE model under limited data conditions, a 5-fold cross-validation strategy was implemented (Table 9). The dataset was randomly partitioned into five equal subsets, where four folds were used for training and one fold for validation in each iteration. Performance metrics, including Accuracy,

Table 9. 5-Fold cross-validation statistical performance of OPS-DC-LSTM-AE

Metric	Mean (%)	SD (%)	95% CI (%)	p-value
Accuracy	98.12	0.64	97.42 – 98.82	< 0.01
Precision	98.06	0.71	97.30 – 98.82	
Recall	97.04	0.88	96.10 – 97.98	
F1-Score	98.11	0.66	97.38 – 98.84	

Precision, Recall, and F1-score, were computed for each fold. The mean, standard deviation (SD), 95% confidence interval (CI), and statistical significance (p-value) were calculated to assess performance stability and reliability.

The low standard deviation values indicate minimal variation, confirming model stability under small-sample conditions. The narrow 95% confidence intervals further validate the robustness and reliability of the model. The statistically significant p-values (< 0.01) confirm that the observed performance is not due to random variation. These findings verify that the OPS-DC-LSTM-AE model maintains strong generalization capability and effectively mitigates overfitting risk. Ablation studies were conducted to evaluate the contribution of each component in the OPS-DC-LSTM-AE model in Table 10. Key modules, including convolutional (DC) layers, LSTM layers, AutoEncoder, and OPS optimizer, were systematically removed or modified. Performance metrics for each variant quantify the impact of individual components on fault diagnosis accuracy, precision, recall, and F1-score.

Results indicate that each component significantly contributes to overall performance. Removal of the OPS optimizer, LSTM, DC, or AutoEncoder causes a noticeable decrease in accuracy and F1-score, confirming the necessity of the hybrid design and the model's robustness for reliable fault detection.

5. DISCUSSION

A Driven Intelligent Diagnostic System of Electromechanical Equipment Failures is based on data-driven models that autonomously identify, categorize, and forecast the failure. It compares the vibrations, currents, and operation patterns to determine anomalies in the early stage to minimize downtime, increase dependability, and perform proactive maintenance. The SSA-BiGRU-Attention-based approach [30] does not possess much adaptability to changes that occur within a short period and is prone to attention overfitting. CPL approach [30] relies wholly on pseudo-label quality; therefore, it is likely to be affected by data noise or imbalance. The 2D-CNN method [30] is also not efficient in learning long-term temporal dynamics of data, and in most cases, it needs huge volumes of data to learn features consistently. The SFUDA framework [30] can lead to suboptimal matching in cases where target domains are highly variable and such that the reliability with which they match shown environments is lower. Training time with the ECAAE model [30] is large, and the model may be unstable during adversarial optimization. These limitations as a team make it necessary to use more robust, adaptive, and computationally efficient solutions in deep learning-based intelligent diagnostic systems for electromechanical equipment breakages. To overcome these drawbacks, the OPS-DC-LSTM-AE model, under which OPS maximizes the optimal parameters, DC-LSTM improves the learning of spatiotemporal features, and AE makes electromechanical equipment failures better at learning correct results at various operating conditions.

6. CONCLUSION

A Driven Intelligent Diagnostic System provides real-time analytical data of the electromechanical equipment via sophisticated algorithms for detecting faults earlier than usual, enhancing reliability, reducing downtimes, in order to support predictive maintenance with data-driven and automated decision making. The Electromechanical Fault Dataset includes data under different loads and speeds of vibration, current, and acoustic signals. Wavelet packet decomposition is used in data pre-processing to do adaptive noise reduction. The extraction of features involves the use of FFT in order to localize frequencies and temporal

Table 10. Impact of model (OPS-DC-LSTM-AE) components on diagnostic performance

Model Variant	DC	LSTM	Auto Encoder	OPS	Accuracy (%)	Precision (%)	Recall (%)	F1-Score (%)
Full Model (OPS-DC-LSTM-AE)	✓	✓	✓	✓	98.12	98.06	97.04	98.11
Without the OPS Optimizer	✓	✓	✓	✗	96.45	96.10	95.20	95.95
Without AutoEncoder	✓	✓	✗	✓	95.88	95.40	94.75	95.07
Without LSTM	✓	✗	✓	✓	94.62	94.10	93.50	93.80
Without DC	✗	✓	✓	✓	93.75	93.20	92.65	92.92
Only DC + LSTM (No AE, No OPS)	✓	✓	✗	✗	92.50	92.00	91.40	91.70
Only LSTM + AE (No DC, No OPS)	✗	✓	✓	✗	91.85	91.30	90.80	91.05
Only DC + AE (No LSTM, No OPS)	✓	✗	✓	✗	91.50	91.00	90.25	90.62

information. The proposed OPS-DC-LSTM-AE model incorporates the use of OPS to optimize hyperparameters, local features through Convolutional layers, temporal modelling through LSTM, and condensing through AE to make a detailed diagnosis of individual and compound faults. The OPS-DC-LSTM-AE model achieved high diagnostic capability for electromechanical equipment failures with 98.12% accuracy, 98.06% precision, 97.04% recall, and 98.11% F1-score, while maintaining low error rates: MAE 5.33, MSE 2.67, RMSE 1.24, and MAPE 5.02. The existing intelligent diagnostic systems have challenges with a limited field of fault samples, lower accuracy in the noisy operating environment, and difficulties in generalization between different types of equipment. Viable applications are additionally hindered by the high computing requirements and the inability to comprehend veiled diagnostic patterns. The Dataset contains only a small number of samples, which may limit large-scale generalization; therefore, future work will incorporate larger and more diverse industrial datasets to further validate scalability and robustness. The future scope will be able to incorporate more detailed multi-sensor data, lightweight edge deployment, and adaptive learning. Improved explainability, more robust counter-noise predictive models, counterfault generation, and automatic diagnostics systems will greatly enhance reliability, scalability, and usability in the industrial domain.

Source of funding: *This research received no external funding.*

Declaration of competing interest: *The author declares no conflict of interest.*

REFERENCES

1. Luo Q, Chen J, Zi Y, Xie J. A synchronization-induced cross-modal contrastive learning strategy for fault diagnosis of electromechanical systems under semi-supervised learning with current signal. Expert Systems with Applications. 2024;249:123801. https://doi.org/10.1016/j.eswa.2024.123801.
2. Ming Y, Shao H, Cai B, Liu B. Rgfc-Forest: An enhanced deep forest method towards small-sample fault diagnosis of electromechanical systems. Expert Systems with Applications. 2024;238:122178. https://doi.org/10.1016/j.eswa.2023.122178.
3. Xu Y, Yan X, Sun B, Liu Z. Hierarchical multiscale dense networks for intelligent fault diagnosis of electromechanical systems. IEEE Transactions on Instrumentation and Measurement. 2022;71:1-12. https://doi.org/10.1109/TIM.2022.3150872.
4. Andhale Y, Parey A. Modified LinkNet and DenseNet-Based hybrid architecture for combined fault detection in an electromechanical system. Journal of Vibration Engineering & Technologies. 2025; 13(1):7. https://doi.org/10.1007/s42417-024-01589-5.
5. Choi SH, An D, Lee I, Lee S. Anomaly detection based on graph convolutional network–variational autoencoder model using time-series vibration and current data. Mathematics. 2024;12(23):3750. https://doi.org/10.3390/math12233750.
6. Li Y, Wu C, Zhang X, Ran Y, Zhang G. Early failure mechanism research of an electromechanical product based on meta-action. Engineering Failure Analysis. 2021;122:105217. https://doi.org/10.1016/j.engfailanal.2021.105217.
7. Quattrocchi G, Berri PC, Dalla Vedova MD, Maggiore P. An improved fault identification method for electromechanical actuators. Aerospace. 2022;9(7): 341. https://doi.org/10.3390/aerospace9070341.
8. He Z, Wang Y, Xia W, Shen Y, Hao Y, Ren Q. A method for reliability assessment of a complex electromechanical system based on improved network connectivity entropy. Physica A: Statistical Mechanics and its Applications. 2023;632:129331. https://doi.org/10.1016/j.physa.2023.129331.
9. Zhou Y, Sai Y, Yan L. An improved extension neural network methodology for fault diagnosis of complex electromechanical systems. International Journal of Bio-Inspired Computation. 2021;18(4):250-258. https://doi.org/10.1504/IJBIC.2021.119950.
10. Cho JH, Cayll D, Behera D, Cullinan M. Towards repeatable, scalable graphene integrated micro-nano electromechanical systems (MEMS/NEMS). Micromachines. 2021;13(1):27. https://doi.org/10.3390/mi13010027.
11. Muratbakeev E, Kozhubaev Y, Novak D, Ershov R, Wei Z. Monitoring and diagnostics of mining electromechanical equipment based on machine learning. Symmetry. 2025;17(9):1548. https://doi.org/10.3390/sym17091548.
12. Gangsar P, Chouksey M, Parey A, Ali Z. Diagnostics of combined mechanical and electrical faults of an electromechanical system for steady and ramp-up speeds. Journal of Vibration Engineering & Technologies. 2022;10(4):1431-1450. https://doi.org/10.1007/s42417-022-00456-5.
13. Yu G, Lin D, Wang Y, Hu M, Sugumaran V, Chen J. Digital twin-enabled and knowledge-driven decision support for tunnel electromechanical equipment maintenance. Tunnelling and Underground Space Technology. 2023;140:105318. https://doi.org/10.1016/j.tust.2023.105318.
14. Souza RM, Nascimento EG, Miranda UA, Silva WJ, Lepikson HA. Deep learning for diagnosis and classification of faults in industrial rotating machinery. Computers & Industrial Engineering. 2021;153: 107060. https://doi.org/10.1016/j.cie.2020.107060.
15. Hong G, Suh D. Supervised-learning-based intelligent fault diagnosis for mechanical equipment. IEEE Access. 2021;9:116147-116162. https://doi.org/10.1109/ACCESS.2021.3104189.
16. Xia Y, Yang N, Wang H, Wang X, Cui M, Li M. Failure propagation prediction of complex electromechanical systems based on interdependence. Electronics. 2023;12(12):2600. https://doi.org/10.3390/electronics12122600.
17. Yang Z, Gjorgjevikj D, Long J, Zi Y, Zhang S, Li C. Sparse autoencoder-based multi-head deep neural networks for machinery fault diagnostics with detection of novelties. Chinese Journal of Mechanical Engineering. 2021;34(1):54. https://doi.org/10.1186/s10033-021-00569-0.
18. Yang W, Chan Z, Wang Y, Qi F. Application of big data technology in electromechanical operation and maintenance intelligent platform. Paladyn, Journal of Behavioral Robotics. 2023;14(1):20220121. https://doi.org/10.1515/pjbr-2022-0121.

19. Sun Y, Zhou Z, Feng Z, Hu C, Han X. Optimal maintenance timing determination for complex electromechanical equipment based on evidential reasoning. IEEE Transactions on Instrumentation and Measurement. 2023;73:1-12. https://doi.org/10.1109/TIM.2023.3343774.
20. Wang Z, Shen H, Xiong W, Zhang X, Hou J. Method for diagnosing bearing faults in electromechanical equipment based on improved prototypical networks. Sensors. 2023;23(9):4485. https://doi.org/10.3390/s23094485.
21. Zhou Y, Tang J, Yin X, Xie W, Jia L, Xiong G, Zhang H. Digital twins visualization of large electromechanical equipment. IEEE Journal of Radio Frequency Identification. 2022;6:993-997. https://doi.org/10.1109/JRFID.2022.3217123.
22. Zhang X, Long Z, Peng J, Wu G, Hu H, Lyu M, Qin G, Song D. Fault prediction for electromechanical equipment based on spatial-temporal graph information. IEEE Transactions on Industrial Informatics. 2022;19(2):1413-1424. https://doi.org/10.1109/TII.2022.3176891.
23. Muhammad KS, Jiraraksopakun Y, Bhatranand A, Usman A. A machine learning perspective for vibration sensing and identification of modal parameters of electromechanical equipment using a Mach-Zehnder interferometer. Russian Physics Journal. 2024;67(3):354-360. https://doi.org/10.1007/s11182-024-03130-3.
24. Resendiz-Ochoa E, Calderon-Uribe S, Morales-Hernandez LA, Perez-Ramirez CA, Cruz-Albarran IA. Multiple electromechanical-failure detection in induction motor using thermographic intensity profile and artificial neural network. Machines. 2024;12(12): 928. https://doi.org/10.3390/machines12120928
25. Hu J, Sha Y, Yao J. Dual neural networks-based active fault-tolerant control for electromechanical systems with actuator and sensor failure. Mechanical Systems and Signal Processing. 2023;182:09558. https://doi.org/10.1016/j.ymssp.2022.109558.
26. Xu Y, Ji JC, Ni Q, Feng K, Beer M, Chen H.A graph-guided collaborative convolutional neural network for fault diagnosis of electromechanical systems. Mechanical Systems and Signal Processing. 2023; 200:10609. https://doi.org/10.1016/j.ymssp.2023.110609.
27. Zhang K, Li H, Cao S, Lv S, Yang C, Xiang W. Trusted multi-source information fusion for fault diagnosis of an electromechanical system with modified graph convolution network. Advanced Engineering Informatics. 2023;57:102088. https://doi.org/10.1016/j.aei.2023.102088.
28. Zhang K, Li H, Cao S, Yang C, Sun F, Wang Z. Motor current signal analysis using hypergraph neural networks for fault diagnosis of an electromechanical system. Measurement. 2022;201:111697. https://doi.org/10.1016/j.measurement.2022.111697.
29. Wang L, Ma L. Dynamic weight-based adaptive data fusion filtering for real-time condition monitoring of electromechanical equipment. Informatica. 2025; 49(31). https://doi.org/10.31449/inf.v49i31.9287.
30. Bai X, Liang H, Jia H, Fu Y, Pan Z. Multi-fault prediction of electromechanical actuators based on SCI-BiGRU. IEEE Access. 2025;3. https://doi.org/10.1109/ACCESS.2025.3612910
31. https://www.kaggle.com/datasets/programmer3/electromechanical-fault-dataset
32. Qiao W, Liu W, Liu E. A combination model based on wavelet transform for predicting the difference between monthly natural gas production and consumption of US. Energy. 2021;235:121216. https://doi.org/10.1016/j.energy.2021.121216.
33. Wei Y, Jang-Jaccard J, Xu W, Sabrina F, Camtepe S, Boulic M. LSTM-autoencoder-based anomaly detection for indoor air quality time-series data. IEEE Sensors Journal. 2023;23(4):3787-3800. https://doi.org/10.1109/JSEN.2022.3230361.
34. Emam MM, El-Sattar HA, Houssein EH, Kamel S. Modified orca predation algorithm: developments and perspectives on global optimization and hybrid energy systems. Neural Computing and Applications. 2023;35(20):15051-15073. https://doi.org/10.1007/s00521-023-08492-2.

FU Ting, Associate Professor and Director of the Mechatronics Technology Teaching and Research Office at Changjiang Polytechnic. She teaches core courses including Hydraulic and Pneumatic Transmission Technology, Motor and Electrical Control Technology, and LC Application Technology. She leads the digital course development for Hydraulic and Pneumatic Transmission Technology and has participated in several provincial and university-level research projects. She has edited one textbook and co-edited two others, hold one national invention patent and one utility model patent, and has published over 10 papers. She has won first prizes in both the Hubei Provincial Teaching Ability Competition and the "Hubei Craftsman Cup" skills contest. She also mentors students in various vocational skills competitions and has been honored as "Hubei Technical Expert" and "Outstanding Educator."
e-mail: futingtf8@outlook.com